# High-Resolution Electron Microscopy of Copper Chromate and the Products of Its Thermal Decomposition

OLAF MARKS AND JOHN R. GÜNTER*

*Institute for Inorganic Chemistry, University of Zürich, Winterthurerstrasse 190, CH-8057 Zürich, Switzerland*

Copper chromate and its thermal decomposition products have been investigated by thermogravimetry, X-ray powder and single-crystal diffraction, and high-resolution electron microscopy in order to study the micromorphology of the intermediate two-phase product, consisting of $CuCr_2O_4$ and $CuO$, known as Adkins catalyst, and the mechanism of its formation. Both steps of the thermal decomposition of $CuCrO_4$ to $CuCr_2O_4$ + $CuO$ and to $CuCrO_2$ are topotactic. $CuO$ forms in minute inclusions (diameters 5–10 nm) coherently embedded in a twinned $CuCr_2O_4$ matrix. © 1988 Academic Press, Inc.

## Introduction

Copper chromium oxides represent well-known heterogeneous catalysts for oxidation/reduction of various organic materials and for the low temperature oxidation of carbon monoxide. Since their introduction into catalysis by Adkins et al. (1, 2), they have been intensively studied by thermoanalytical (3–7) and spectroscopical (8, 9) methods. Whereas the crystal structures of the pure phases $CuCrO_4$ (10, 11), $CuCr_2O_4$ (12–14), $CuO$ (15, 16), and $CuCrO_2$ (17, 18) are all known, no data exist for the real structure of mixed oxides or oxide mixtures as used in catalysis. However, chemical properties of solids strongly depend on their micromorphology, i.e., particle sizes, aggregates, intergrowths, and crystallographic orientation relations due to possible topotactic formation. Practical Adkins catalysts may vary in their Cu:Cr

ratio, in dependence of their preparation and precursors. They usually contain $CuCr_2O_4$ and $CuO$ and are frequently prepared by thermal decomposition of $CuCrO_4$, which may be the starting material or an intermediate product of catalyst preparation. For the activation of the catalysts, these are reduced in hydrogen, which produces metallic copper from $CuO$, embedded either in $CuCr_2O_4$ (19) or in $CuCrO_2$ (6). Obviously, the micromorphology of these inclusions of $CuO$ must have a decisive influence on the properties of the catalysts. We have therefore studied it by means of high-resolution electron microscopy in combination with other techniques (20). The results also shed light on the mechanism of thermal decomposition of $CuCrO_4$.

## Experimental

### Preparation

*$CuCrO_4$ single crystals.* Single crystals of copper(II) chromate for X-ray diffraction

---

* To whom correspondence should be addressed.

15

have been prepared according to a modification of the procedure given in (21) as follows: 35 g (350 mmole) of $CrO_3$ (Merck p.a.) were dissolved in 25 ml of distilled water; 20 g (90 mmole) of $Cu(CO_3) \cdot Cu(OH)_2$ (Merck puriss.) were added in small portions. The mixture was put in a closed Pyrex tube after the end of the $CO_2$-evolution and held at 210–220°C for about 20 days. The product was filtered, washed with water, and dried in a dessiccator. Product crystals were dark red to black elongated platelets of up to 0.3 mm in length.

*Finely divided $CuCrO_4$ for electron microscopy.* For the preparation of finely divided $CuCrO_4$ the above procedure was modified as follows: The reaction mixture was kept in a closed Pyrex tube at 85°C for 4 days. The yield is small, but cannot be increased without increase in particle size, which amounts to approximately 800 nm in length.

*$CuCr_2O_4$.* Single crystals could not be obtained. Finely divided samples for comparison were prepared by a method modified from the literature (22): 4.00 g (10 mmole) of $Cr(NO_3)_3 \cdot 9H_2O$ (Fluka p.a.) and 2.44 g (10.1 mmole) of $Cu(NO_3)_2 \cdot 3H_2O$ (Fluka p.a.) were dissolved in 25 ml ethanol each, mixed, and evaporated to dryness. This mixture was decomposed at 250–300°C in air, yielding a fine powder of CuO and $Cr_2O_3$, which was added to a flux of $CuCl_2$, melted at 640°C in an alumina crucible, and left at this temperature in air for 12 hr. After cooling, excess $CuCl_2$ was dissolved with water, and the product was purified from CuO with HCl, centrifuged, and dried at 100°C. The irregularly shaped crystallites were black and up to 200 nm long.

*CuO.* Finely divided copper(II) oxide was obtained from the thermal decomposition of $Cu(NO_3)_2 \cdot 3H_2O$ (Merck p.a.) in air at 250–300°C. Crystallites were black and measured 50–500 nm.

*$CuCrO_2$ single crystals.* Crystalline Cu CrO₂ was prepared according to (23) in the form of hexagonal platelets up to 2 mm in diameter.

*Finely divided $CuCrO_2$.* $CuCrO_2$ powders were prepared by thermal decomposition of finely divided $CuCrO_4$ and 650°C under nitrogen.

### Thermogravimetry

Thermogravimetric experiments were performed on Perkin–Elmer TGS-2, Mettler TA-1, and Mettler TA 2000C instruments.

### X-Ray Diffraction

X-ray diffraction of powders was performed using a Type FR 552 Guinier–IV camera (Nonius, Delft) with monochromatized $CuK\alpha_1$ radiation. Single-crystal and pseudo-single-crystal diffractograms were recorded with Precession cameras of Nonius, Delft, and Stoe & Cie, Darmstadt, with $MoK\alpha$ radiation.

### Electron Microscopy

All transmission electron micrographs were recorded on a JEOL JEM 200-CX microscope with ultra high-resolution pole piece ($C_s$ = 1.2 mm), top entry double tilt goniometer, and SIEMENS image intensifier. As specimens, only material prepared in finely divided form (see above) was used, in order to avoid artifacts from grinding. Samples were suspended in water or ethanol by ultrasonic treatment (1 MHz), put on holey carbon films, and dried in air. Optical diffraction of the photographic negatives was performed on an optical bench with a laser (24). High-resolution image simulation was done using the EMS program system (25).

## Results

### Thermal Decomposition of $CuCrO_4$

The thermal decomposition of $CuCrO_4$ in a nitrogen atmosphere occurs in two steps.
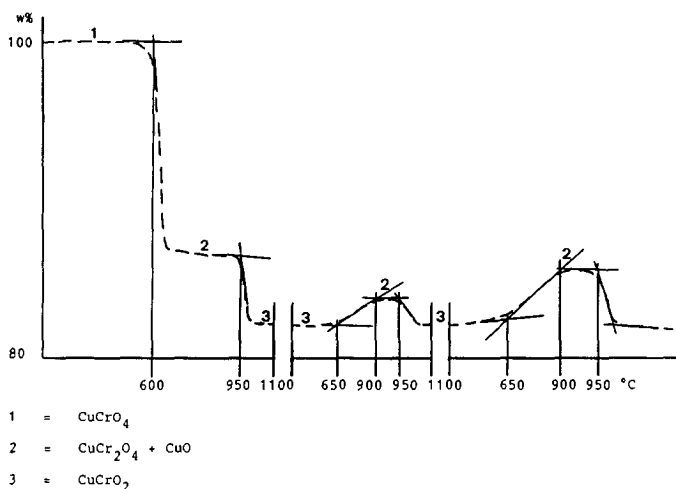
FIG. 1. Thermogravimetrical decomposition curve of $CuCrO_4$ in an oxygen atmosphere, and the effect of cyclic cooling and reheating.

At first, above about 500°C oxygen is lost, and the monophasic starting material is transformed into a two-phase mixture of $CuCr_2O_4$ and CuO, which reacts above about 750°C to the again monophasic end product $CuCrO_2$. The intermediate occurrence of a mixture of $Cr_2O_3$ and CuO postulated from ESR measurements (9) has not been observed in our experiments, neither by X-ray diffraction nor by selected area electron diffraction. If the thermal decomposition occurs in pure oxygen, the reaction path is the same as in nitrogen, but the reaction temperatures are considerably higher, i.e., 600°C for the first and 950°C for the second step. Independently from the atmosphere, both steps are rapid, indicating a mechanism requiring only moderate diffusion of component ions and an intimate contact between the solid particles.

If the final product, $CuCrO_2$, is cooled and reheated under oxygen, it takes up oxygen again at 650°C and loses it again at 950°C. After two such cooling/heating cycles at cooling/heating rates of 10°/min, the second step of the reaction is fully reversible and again remarkably fast (Fig. 1). The products of such cycles were identified by

X-ray powder diffraction as $CuCr_2O_4$ and CuO.

## $CuCrO_4$ and the Formation of $CuCr_2O_4$

The crystal structure of $CuCrO_4$ consists of corner-sharing, tetragonally elongated $CuO_6$ octahedra, linked by slightly deformed $CrO_4$ tetrahedra. The oxygen anions form a slightly distorted, nearly cubic close-packed sublattice. It is orthorhombic, space group Cmcm, $a = 0.5433$ nm, $b = 0.8968$ nm, $c = 0.5890$ nm, $Z = 4$ (10, 11).

$CuCr_2O_4$ is a deformed spinel with a tetragonally distorted cubic close-packed anion sublattice, Cr occupying the octahedral and Cu the tetrahedral interstices. Space group $I\overline{4}2d$, $a = 0.604$ nm, $c = 0.778$ nm, $Z = 4$ (12–14).

High-resolution electron micrographs show that the crystals of $CuCrO_4$ are well ordered (Fig. 2). After partial thermal decomposition, both single-crystal Precession photographs and selected area electron diffraction patterns reveal the presence of highly oriented $CuCr_2O_4$ as reaction product. CuO, however, cannot be detected by these methods, contrary to powder X-ray diffraction, which clearly indicates the
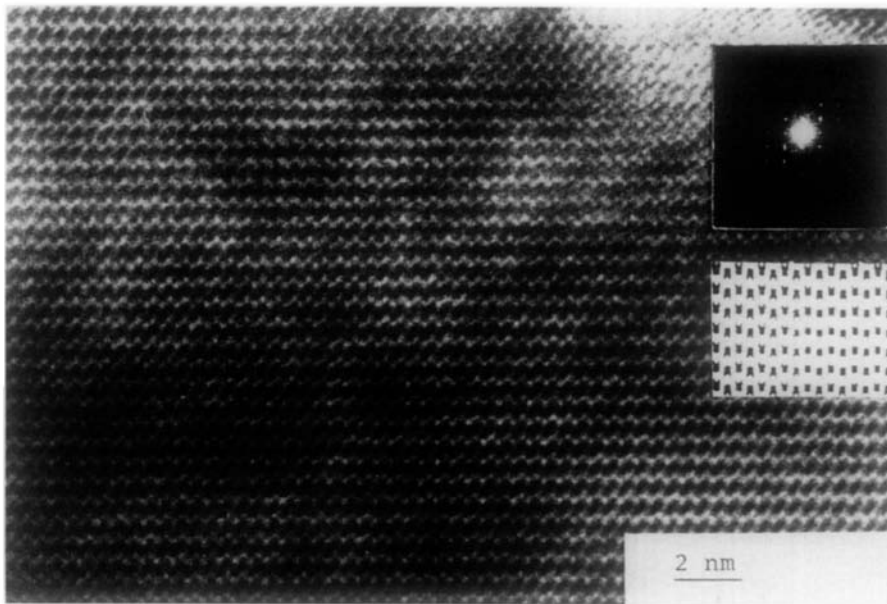
FIG. 2. High-resolution electron micrograph of a $CuCrO_4$ crystal. Insets: Optical diffraction pattern and computer simulated image.

presence of this phase, although in a poorly crystalline state. Samples of $CuCrO_4$ strongly irradiated by electrons decompose in an analogous way, the reaction starting from the surfaces and proceeding to the in- terior of the crystals. The selected area electron diffraction pattern of such a partly decomposed crystal shows the relative ori- entation of $CuCrO_4$ and $CuCr_2O_4$; $CuO$ is again not detected (Fig. 3). The reason for
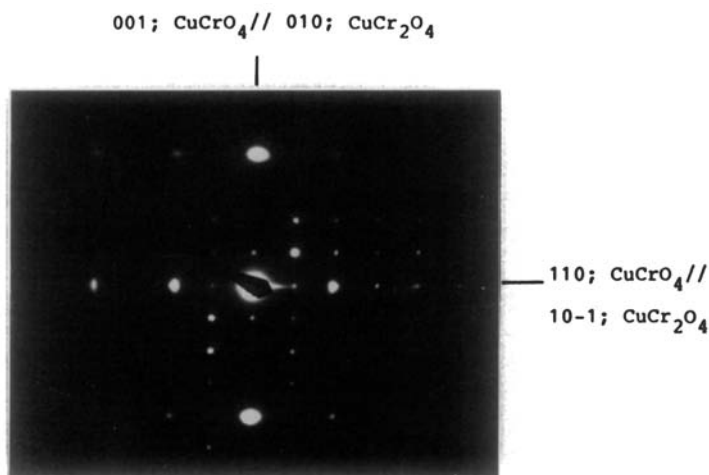


FIG. 3. Selected area electron diffraction pattern of a crystal of $CuCrO_4$ partly decomposed in the electron beam. Indexing for both $CuCrO_4$ and $CuCr_2O_4$.

this may be an overlap of CuO reflections with those of the other two phases (an argument supported strongly by Figs. 6 and 7), a lack of intensities due to very small particle size, or a combination of both.

The topotactic orientation relations between $CuCrO_4$ and $CuCr_2O_4$ deduced from these diffraction experiments are the following:

$$a_{CuCr_2O_4} \text{ parallel to } a_{CuCrO_4},$$
$$b_{CuCr_2O_4} \text{ parallel to } c_{CuCrO_4}, \text{ and}$$
$$c_{CuCr_2O_4} \text{ parallel to } -b_{CuCrO_4}.$$

In addition to this cell transformation, the lengths of the cell axes are changed by $+10.0\%$ for $a$, $-15.1\%$ for $b$, and $+2.5\%$ for $c$, referring to the unit cell of $CuCrO_4$.

This lattice distortion, caused by the displacement of metal cations within the oxygen sublattice, results almost in a coincidence of the planes $(201)_{CuCr_2O_4}$ with $(310)_{CuCrO_4}$. Furthermore, the lowering of the symmetry induces a threefold twinning of the product $CuCr_2O_4$, which can be described by rotations of $60°$ around the $[\bar{2}01]$ zone axis of $CuCr_2O_4$. The presence of this threefold twinning was later confirmed by direct electron microscopic lattice imaging.

*Localization of CuO*

The crystal structure of CuO differs from those of $CuCrO_4$ and $CuCr_2O_4$ in that it is not derived from a close-packed oxygen lattice, but consists of crossed bands of square planar coordinated copper(II) ions. It is monoclinic, $a = 0.46837$ nm, $b = 0.34226$ nm, $c = 0.51288$ nm, $\beta = 99.54°$, space group $C2/c$ *(15, 16)*. Nevertheless, its diffraction reflections correspond to $d$ values, which may be coincident with reflections of $CuCr_2O_4$, and thus it may not uniquely be identified by selected area electron diffraction, although its presence is evident from powder X-ray diffraction. The only means of localizing it in the decomposed product is therefore high-resolution electron mi-
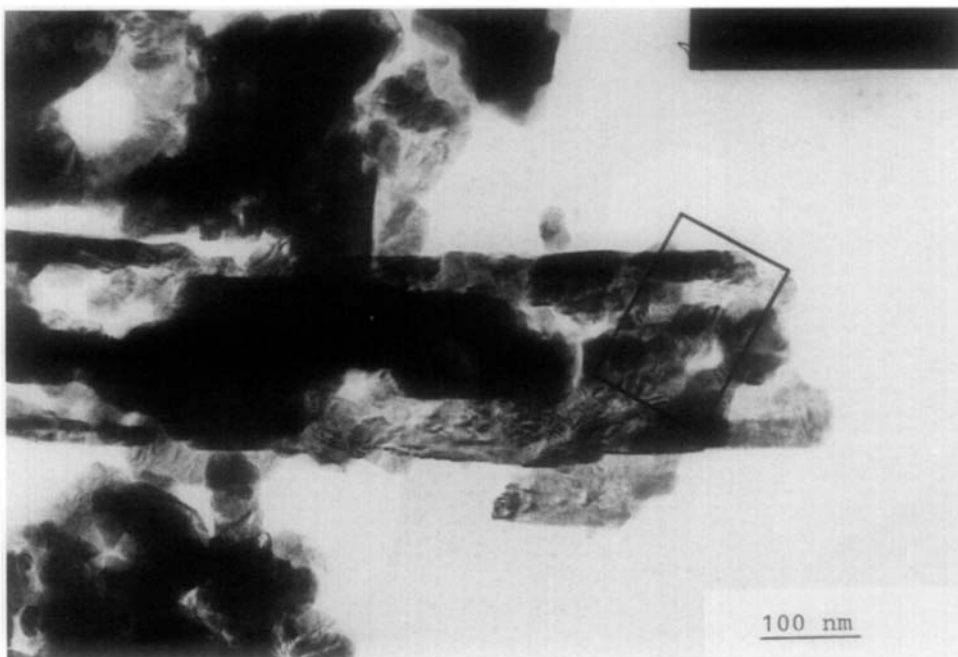


FIG. 4. Overview of a $CuCrO_4$ particle thermally decomposed to $CuCr_2O_4$ and CuO.
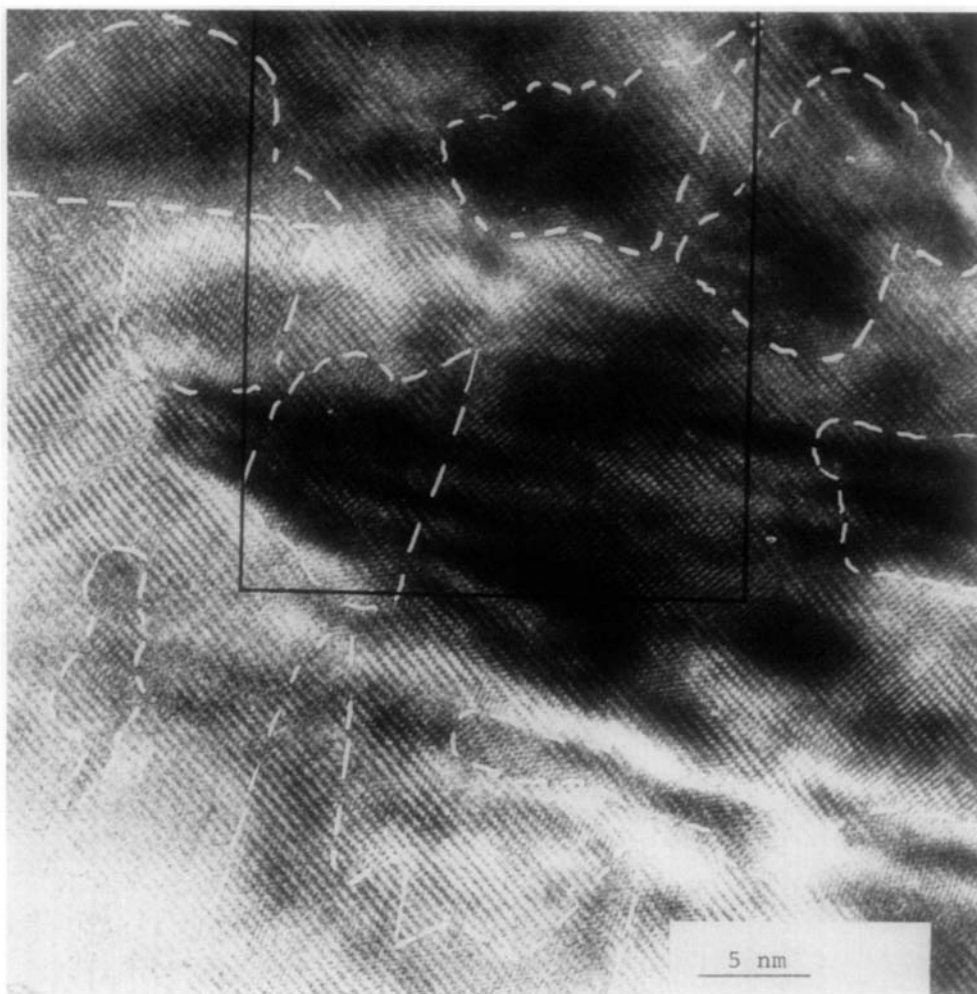
FIG. 5. High-resolution electron micrograph of CuO areas (marked with white lines) embedded in a matrix of $CuCr_2O_4$. Black rectangle, see Fig. 6.

croscopy. Dark field electron microscopy is hardly applicable, due to the near coincidence of the reflections of the two phases (cf. Fig. 7). Figure 4 shows that the particles containing $CuCr_2O_4$ and CuO, conserve as a whole their original shape, although they are now rather porous. This is due to the loss of oxygen during the first step of decomposition, but there are still extended, continuous domains of crystalline material. At higher magnification, it can be seen that these large domains are

essentially $CuCr_2O_4$ in a multiply twinned form, with partly very small sizes of the individual twins. Embedded in this matrix, CuO can now be localized. An unambiguous identification is only possible in areas of 5–10 nm in diameter, where CuO exhibits crossed lattice fringes, which can be identified by optical diffraction and by image simulation (Figs. 5 and 6). Consequently, the selected area electron diffraction patterns can now be indexed for both phases present, as shown for an exam-
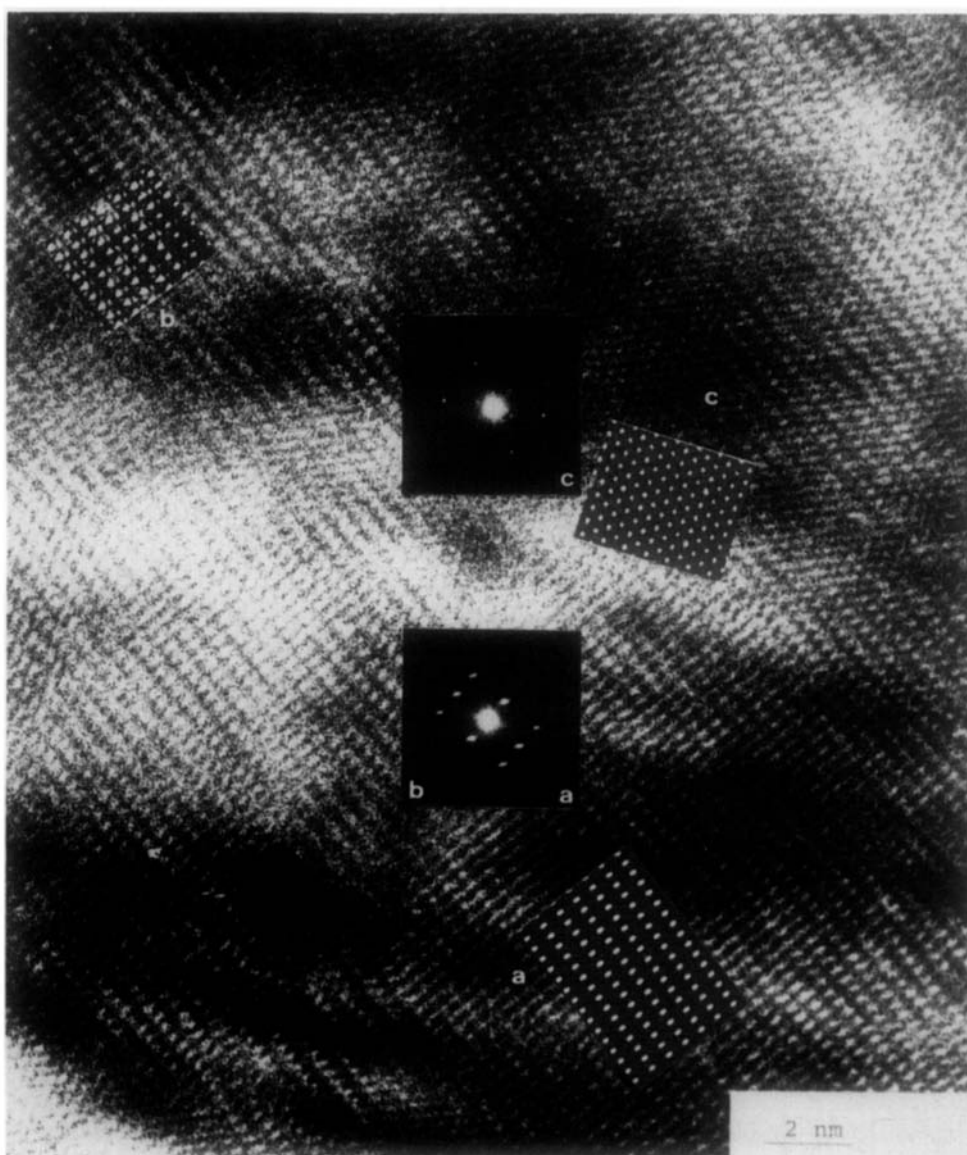
FIG. 6. Enlarged portion of the micrograph in Fig. 5. a, $CuCr_2O_4$ in [101] orientation; b, $CuCr_2O_4$ in [$\bar{1}$31] orientation; c, CuO in [0$\bar{1}$1] orientation. Insets: optical diffraction patterns and simulated images.

ple in Fig. 7. Finally, this localization of CuO also allows the topotactic orientation relations to be deduced, both relative to $CuCr_2O_4$ and to the parent $CuCrO_4$:

$$(100)_{CuO} \text{ parallel to } (\overline{1}01)_{CuCr_2O_4} \text{ parallel to } (\overline{1}\,\overline{1}0)_{CuCrO_4},$$
$$(010)_{CuO} \text{ parallel to } (1\,\overline{1}\,\overline{1})_{CuCr_2O_4} \text{ parallel to } (\overline{1}1\overline{1})_{CuCrO_4},$$
$$(001)_{CuO} \text{ parallel to } (1\overline{1}1)_{CuCr_2O_4} \text{ parallel to } (1\overline{1}\,\overline{1})_{CuCrO_4}.$$

## Formation of $CuCrO_2$

The second step of the thermal decomposition of $CuCrO_4$ transforms the two-phase
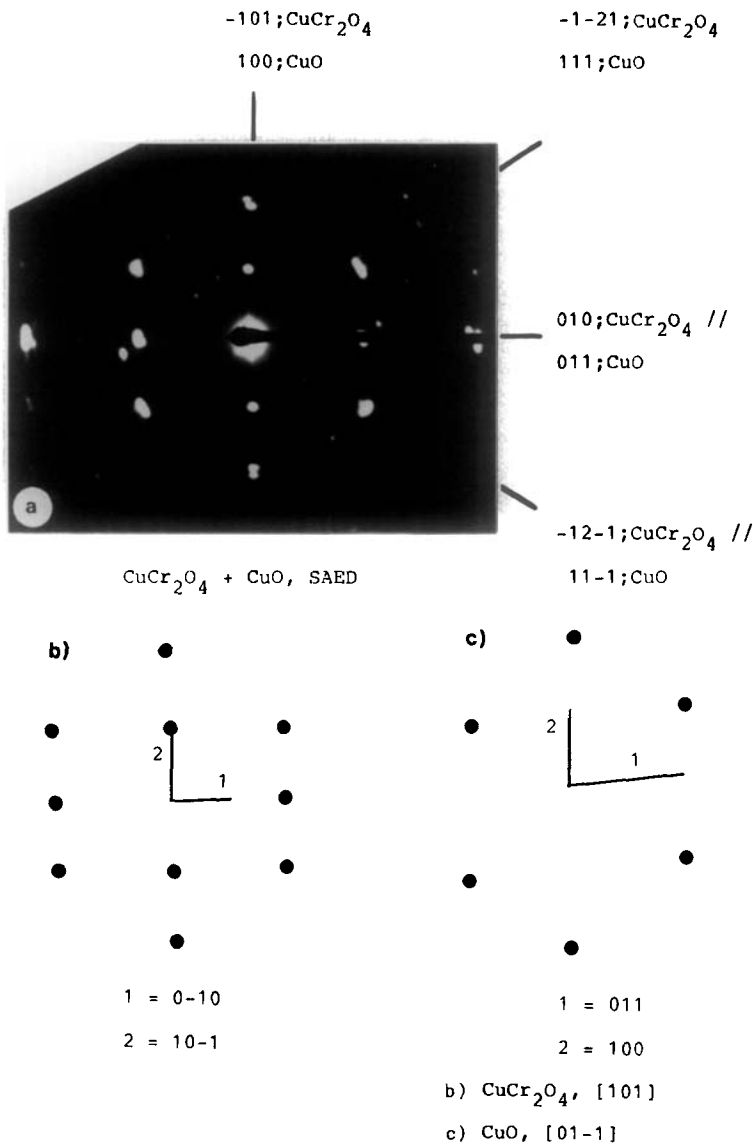
FIG. 7. (a) Selected area electron diffraction pattern of a particle containing $CuCr_2O_4$ and CuO, indexed for both phases. Note near-coincidence of reflections. (b) Simulated diffraction pattern of $CuCr_2O_4$ [101]. (c) Simulated diffraction pattern of CuO [01$\bar{1}$].

intermediate product, consisting of Cu $Cr_2O_4$ and CuO, into another single-phase material, $CuCrO_2$. The latter belongs to the rhombohedral delafossite structure type, with $a = 0.5951$ nm, $\alpha = 28.93°$, $Z = 1$ (17, 18). It can be described as layers of close-packed $CrO_6$ octahedra, linked by linearily coordinated copper(I). This reaction step is, for the finely divided material used for electron microscopic investigations, always linked to sintering, causing the loss of the original particle shapes, as shown in Fig. 8. The product $CuCrO_2$ crystallites are how-ever well ordered, as is evident from high-resolution micrographs, which show no ap-parent crystal defects (Fig. 9). X-ray
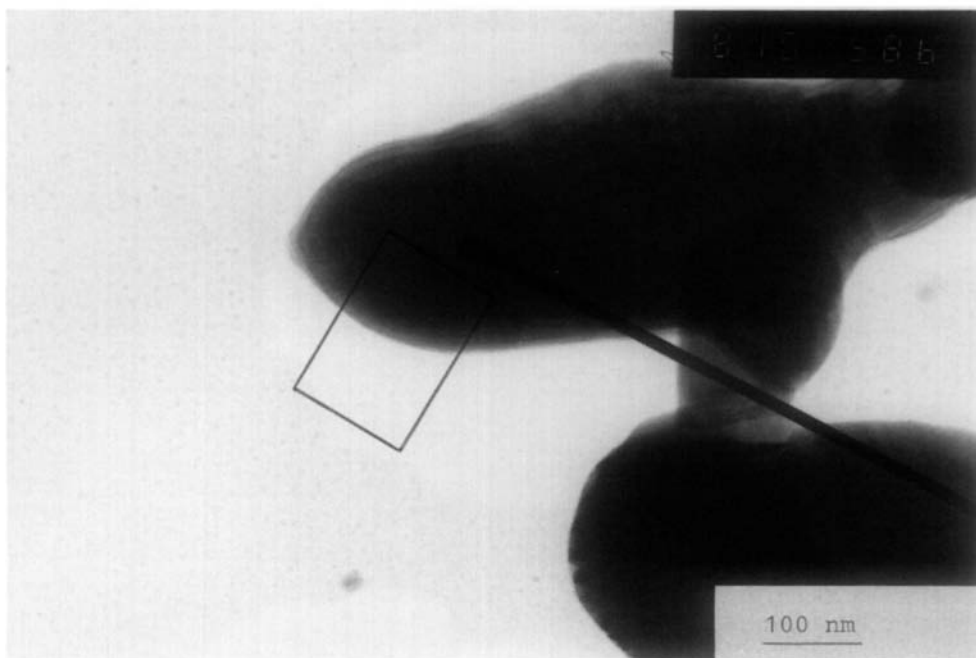
FIG. 8. Overview of CuCrO₂ particles, rounded due to sintering. Black rectangle, see Fig. 9.
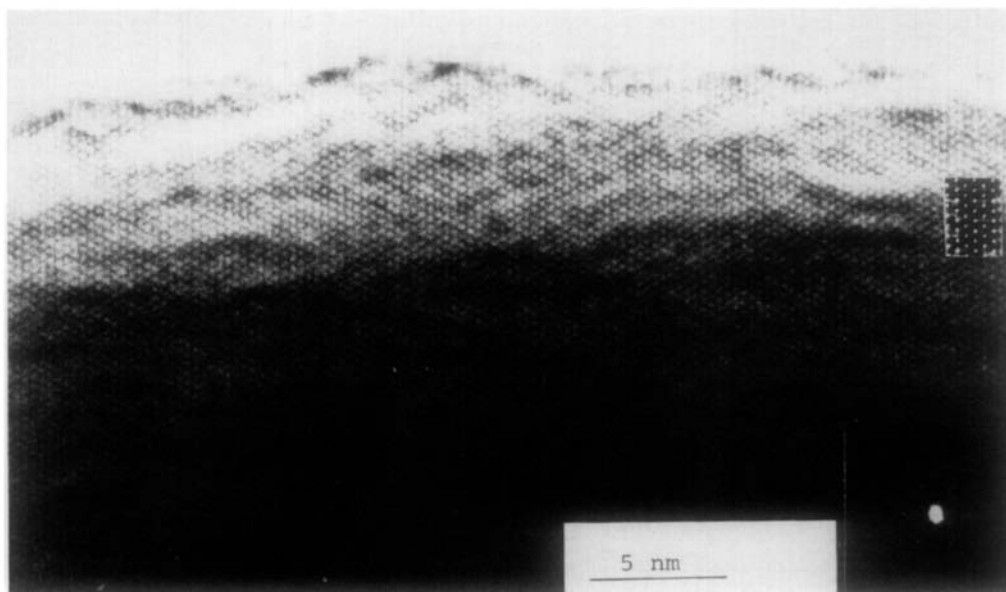


FIG. 9. High-resolution electron micrograph of the border region of a CuCrO₂ particle. Insets: optical diffraction pattern, corresponding to [$\bar{1}11$] and simulated image for this orientation

diffraction patterns taken from decomposed single crystals allow, however, the deduction of topotactic orientation relations also for this step. Thereby, two different product orientations have repeatedly been observed:

Orientation I:

$(\bar{1}10)_{CuCrO_2}$ parallel to $(100)_{CuCr_2O_4}$,
$(1\,\bar{1}0)_{CuCrO_2}$ parallel to $(010)_{CuCr_2O_4}$, and
$(00\bar{1})_{CuCrO_2}$ parallel to $(001)_{CuCr_2O_4}$;

Orientation II:

$(100)_{CuCrO_2}$ parallel to $(100)_{CuCr_2O_4}$,
$(1\bar{2}0)_{CuCrO_2}$ parallel to $(010)_{CuCr_2O_4}$, and
$(10\bar{2})_{CuCrO_2}$ parallel to $(001)_{CuCr_2O_4}$;
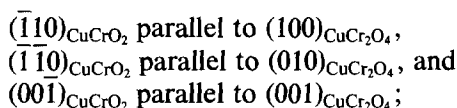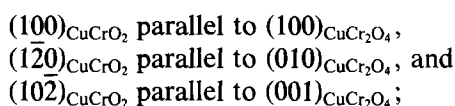
## Summary and Conclusions

The thermal decomposition of $CuCrO_4$ proceeds in two distinct steps, both of which are topotactic. In the first step, $CuCr_2O_4$ and $CuO$ are formed. The latter is not detected on single-crystal X-ray photographs or in selected area electron diffraction, but can unambiguously be localized by high-resolution electron microscopic lattice imaging.

The topotactic process is controlled by the conservation of an essentially cubic close-packed oxygen lattice, in which the metal cations diffuse over short distances only, whereby all cations change their first coordination sphere. The observed systematic threefold twinning of $CuCr_2O_4$ by rotation around the $[20\bar{1}]$ zone axis can be explained by the virtually identical atomic arrangement within the twin planes (112), $(1\bar{1}2)$, and (010). $CuO$ could only be localized by electron microscopy, combined with image simulation and optical diffraction. It is also formed in a topotactic process, involving a more pronounced distortion of the oxygen sublattice, which however does not change its orientation, so that the $CuO$ particles remain coherently connected to the $CuCr_2O_4$ matrix. This cor-

responds to the thermoanalytical result that the reaction proceeds fast and involves only short diffusion paths. The $CuO$ inclusions are minute, with diameters of only 5–10 nm, which probably explains the high catalytic activity of the $CuCrO_4$ decomposition products known as Adkins catalysts. If decomposition is caused by electron bombardment within the electron microscope, it can be observed to start from the crystal surfaces, proceeding to the interior, leaving cracks and pores behind, which act as diffusion pathways for the release of oxygen, leaving the oxygen sublattice intact over relatively large areas. Chromium diffuses into these areas, thus producing a matrix of twinned $CuCr_2O_4$, in which remains the finely dispersed $CuO$. Further decomposition of this two-phase product again proceeds topotactically to form another single-phase material, $CuCrO_2$. In this step, the oxygen sublattice remains unaltered in layers coordinating chromium, whereas the copper is transported into positions in between these layers, under a distinct widening of the oxygen packing. Due to the elevated temperature of this second reaction step, it is accompanied by sintering effects.

The results of these topotactic reaction processes suggest that topotaxy is not a phenomenon restricted to large crystals, but may also be observed in extremely finely divided solids, such as in this case with $CuO$ particles of only 5–10 nm in size, i.e., almost X-ray amorphous. It may be expected that the use of high-resolution electron microscopy for the study of the product micromorphology in addition to diffraction methods will greatly expand the number of reactions of solids recognized to be topotactic.

## References

*1.* H. Adkins and R. Connor, *J. Amer. Chem. Soc.* **53**, 1091 (1931).

2. H. ADKINS, E. E. BURGOYNE, AND H. J. SCHNEIDER, *J. Amer. Chem. Soc.* **72,** 2626 (1950).
3. H. CHARCOSSET, P. TURLIER, AND Y. TRAMBOUZE, *J. Chim. Phys.* **61,** 1249 (1964).
4. L. WALTER-LÉVY AND M. GOREAUD, *Bull. Soc. Chim. France* **3,** 830 (1973).
5. E. G. DEROUANE, Z. GABELICA, AND R. HUBIN, *Thermochim. Acta* **14,** 315 (1976).
6. S. P. TONNER, W. S. WAINWRIGHT, D. L. TRIMM, AND N. W. CANT, *Appl. Catal.* **11,** 93 (1984).
7. K. C. VLACH, Y.-Z. YON, AND Y. A. CHANG, *Thermochim. Acta* **103,** 361 (1986).
8. J. ARSÈNE, M. LENGLET, A. ERB, AND P. GRANGER, *Rev. Chim. Miner.* **15,** 318 (1978).
9. Z. GABELICA, E. G. DEROUANE, AND R. HUBIN, *J. Therm. Anal.* **18,** 315 (1980).
10. K. BRANDT, *Ark. Kemi Mineral. Geol.* **A17**(6), 1 (1943).
11. N. SEFERIADIS, Ph.D. Thesis, University of Zürich, 1986.
12. F. BERTAUT AND C. DÉLORME, *C. R.* **238,** 504 (1951).
13. E. PRINCE, *Acta Crystallogr.* **10,** 554 (1957).
14. J. D. DUNITZ AND L. E. ORGEL, *J. Phys. Chem. Solids* **3,** 20 (1957).
15. S. ASBRINK AND L. J. NORRBY, *Acta Crystallogr. Sect. B* **26,** 8 (1970).
16. G. TUNNELL, E. POSNIAK, AND C. J. KSANDA, *Z. Kristallogr.* **90,** 120 (1935).
17. J. D. STROUPE, *J. Amer. Chem. Soc.* **71,** 569 (1949).
18. W. DANNHAUSER AND P. A. VAUGHAN, *J. Amer. Chem. Soc.* **77,** 896 (1955).
19. H. OHTSUKA, K. AOMURA, N. TOMITA, K. HASHIMOTO, AND O. TAKADA, *Hokkaido Daigaku Kogakubu Iho* **41,** 199 (1966).
20. O. MARKS, Ph.D. Thesis, University of Zürich, 1987.
21. K. LESCHEWSKY AND K. KOTHE, *Z. Anorg. Chem.* **240,** 62 (1939).
22. G. KAINZ AND H. HORWATITSCH, *Z. Anal. Chem.* **177,** 344 (1960).
23. O. KRAUSE AND W. THIEL, *Ber. Dtsch. Ges. Keram.* **15,** 101 (1934).
24. B. E. P. BEESTON, R. W. HORNE, AND R. MARKHAM, "Electron Diffraction and Optical Diffraction Techniques," North-Holland, Amsterdam, 1973.
25. P. A. STADELMANN, *Ultramicroscopy* **21,** 131 (1987).